IOP PUBLISHING JOURNAL OF MICROMECHANICS AND MICROENGINEERING

J. Micromech. Microeng. **19** (2009) 115025 (12pp) doi:10.1088/0960-1317/19/11/115025

A batch-fabricated and electret-free silicon electrostatic vibration energy harvester

P Basset[1], D Galayko[2], A Mahmood Paracha[1], F Marty[1], A Dudka[2] and T Bourouina[1]

[1] Université Paris-Est, ESYCOM Lab., ESIEE Paris, BP 99, 2 bd Blaise Pascal, 93162 Noisy-le-Grand Cedex, France

[2] Université Paris-VI, LIP6 Lab., BP 167, 4 Place Jussieu, 75252 Paris Cedex, France

E-mail: p.basset@esiee.fr

Received 23 July 2009, in final form 10 September 2009
Published 12 October 2009
Online at stacks.iop.org/JMM/19/115025

Abstract

This paper presents a novel silicon-based and batch-processed MEMS electrostatic transducer for harvesting and converting the energy of vibrations into electrical energy without using an electret layer. Effective conversion from the mechanical-to-electric domains of 61 nW on a 60 MΩ resistive load, under a vibration level of 0.25 *g* at 250 Hz, has been demonstrated. Rigorous analysis of the efficiency of the harvester is presented, covering issues related with mechanical and electrical operation. Various schemes for the conditioning electronics are discussed and the harvested power measurements using a dc/dc converter are explained in detail. The paper concludes with a comparison with previous electrostatic transducers based on a new simple factor of merit.

(Some figures in this article are in colour only in the electronic version)

1. Introduction

In our surroundings there are numerous energy sources which can be used for electric energy generation [1, 2], and which are suitable for energizing abandoned sensors. These include ambient radio frequency electromagnetic waves, light, temperature gradient, airflow, mechanical vibrations, heel strike, etc. Ambient vibrations are of special interest [3] as they are available in a broadband vibration spectrum and in various applications like cars, airplanes and helicopters, or buildings and bridges. According to [4], the frequencies of domestic applications like heating, ventilation and air conditioning (HVAC), blenders, washing machines and CD writers lie up to 120 Hz with acceleration ranging from 0.2 m s^{-2} to 10 m s^{-2}. For car engines the vibration spectrum is around 200 Hz with an acceleration of 12 m s^{-2}, whereas for a car compartment it is around 13–33 Hz with an acceleration of around 3–6 m s^{-2} [5]. For a tire pressure monitoring system (TPMS), a frequency range between 5 Hz and 1 kHz and an acceleration ranging from 4000 *g* to 5000 *g* is available [6]. Similarly, vibrations exist in aircraft: for instance, [7] reports a spectrum of noise in a plane cabin with vibration peaks around 100 and at 200 Hz.

The process of electrical power generation from mechanical vibrations can be described in two stages. At first, a proof mass is coupled with the environmental vibrations through an elastic link: the mass and the spring constitute a mechanical resonator present in all vibration energy harvesters (cf figure 1). Thanks to the elastic coupling with the vibrating frame *Ox*, the mass moves in this reference system and the resonator accumulates mechanical energy. The second stage consists of the conversion of this mechanical energy into electric energy. For this purpose, an electromechanical transducer should apply a damping force on the mass, i.e. it should perform a negative work on the mechanical system. The conditioning circuit manages the electrical energy flow so as to accumulate the maximum of energy in the reservoir which supplies the load. Also, the conditioning circuit creates the electrical context necessary for the desired operation of the electromechanical transducer.

In the case of electromagnetic [8, 9], piezoelectric [10–13] and electrostatic [5, 14–16, 26] transducers, the

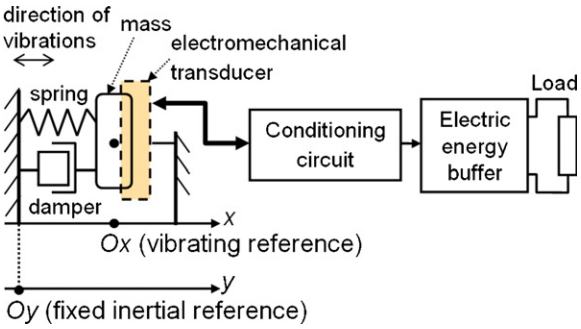

Figure 1. Diagram of the general architecture of a mechanical energy harvester.

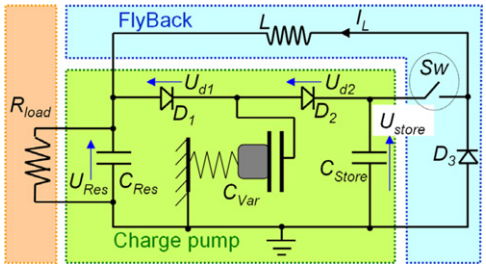

Figure 2. Three-capacitor harvester electrical schematic (from [16]).

damping force is created by a magnetic field, straining piezoelectric material and electric field respectively. More recent approaches use the *Villari effect* in magnetostricitve materials [17] or a combination of piezoelectric and magnetostrictive mechanisms in magnetoelectric composites [18]. Electromagnetic transducers have the best power density but they require ferromagnetic materials and bulky parts. Efficient piezoelectric devices need materials in the form of thin films which are not always compatible with a CMOS process. Electrostatic harvesters, such as those considered in this paper, have a rather lower power density and need an initial pre-charge to start unless they use an electret layer [19–23]. However, such systems are still very attractive since they can be fabricated in a silicon micromachined process compatible with CMOS and are suitable for miniaturization. Most of working electret-free electrostatic vibration energy harvesters (VEH) made of silicon with integrated features are macroscopic devices that use discrete-element technology [16, 24–26].

A promising conditioning circuit for electrostatic electret-free transducers has been proposed in [16]. It consists of a charge pump acting as a one-stage MEMS dc/dc converter that accumulates the energized charges and an inductive flyback circuit that returns the charge pump to a preceding state away from saturation, meanwhile transferring the energy from the charge pump to a tank capacitor. This architecture, shown in figure 2, allows the system to be fully autonomous. In this paper, we detail a similar electromechanical dc/dc converter based on a novel fully integrated silicon MEMS resonant transducer [27, 28]. The system is optimized to be powered by mechanical vibrations at a frequency of 250 Hz. It effectively converts mechanical energy to electrical energy which can

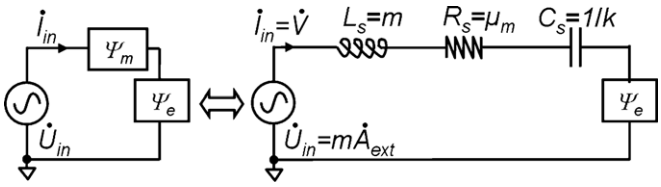

Figure 3. Equivalent electrical network of a spring-mass vibration energy harvester.

be used effectively to feed low-power electronics devices, by increasing the lifetime of a battery in a vibrating environment or by being part of a fully autonomous system for energy harvesting like the one described in [16].

This paper is organized as follows. In section 2, we present a new simple analysis to determine the maximal power that can be harvested in spring-mass systems having a harmonic motion and we discuss various typical conditioning circuits for electret-free electrostatic autonomous generators. In section 3, we present the energy transducer we fabricated and in section 4 we detail the experiment of power conversion from the mechanical-to-electrical domains.

2. Power generation

2.1. Maximal power generation in a spring-mass system with a harmonic motion

Close-form expressions of the maximum power that can be generated from a spring-mass system excited with a sinusoidal force have already been presented in previous papers [29–32]. We present in this section a very simple new analysis based on the analogy with an electrical impedance network.

In the mechanical domain the harvester can be represented by the equivalent electrical network in figure 3, where m, k, A_{ext} and μ_m are mass, spring stiffness, acceleration of external vibrations and mechanical damping, respectively. Ψ denotes the mechanical impedance which is defined from the electromechanical analogy as minus the ratio between the complex amplitude of the force and of the velocity of the point of the force application. Ψ_e is the mechanical impedance of the transducer, and Ψ_m is the mechanical impedance of the resonator which is calculated as

$$\Psi_m = \frac{k}{\mathrm{j}\omega} + \mathrm{j}\omega m + \mu_m. \tag{1}$$

In the energy harvesting literature, the electromechanical transducer is often represented by an ideal damper, i.e. by a dipole with real impedance. However, this representation is very restrictive, and can only be applied to few particular cases. In general, the impedance of the transducer is complex, and the designer must optimize it so that the transducer absorbs the maximal power.

From the electromechanical analogy, the power absorbed by a dipole is the real part of the complex power, defined as the half-square of the module of the current times the impedance of the load. In the mechanical domain, the current is equivalent to the velocity and the mechanical impedance is defined as minus the ratio between the complex amplitudes of force ($\dot{F}$)

and velocity ($\dot{V}$). The power harvested from mechanical-to-electrical domains corresponds to

$$P_h = \tfrac{1}{2}|\dot{V}|^2 \,\mathrm{Re}(\Psi_e). \tag{2}$$

Here and later, the dotted letters denote complex amplitudes of dynamic sinusoidal quantities. The velocity $\dot{V}$ is found from the equivalent electrical network in figure 3.

When designing an energy harvester, it is interesting to know what the maximal amount of power is that can be extracted from a given source of vibrations and a given resonator, and with what load impedance value Ψ_e it can be achieved. In equation (2), both $|\dot{V}|$ and $\mathrm{Re}(\Psi_e)$ have to be maximized, but there is an implicit relation between these two quantities. Let us express this relation. Analyzing the network in figure 3, we have

$$\Psi_m + \Psi_e = \frac{m\dot{A}_{\mathrm{ext}}}{\dot{V}}. \tag{3}$$

Equating the absolute values of both parts and considering $\mathrm{Re}(\Psi_e) + \mathrm{Re}(\Psi_m)$ positive, we get for the real part of Ψ_e:

$$\mathrm{Re}(\Psi_e) = \sqrt{\left(\frac{mA_{\mathrm{ext}}}{V}\right)^2 - [\mathrm{Im}(\Psi_m + \Psi_e)]^2} - \mathrm{Re}(\Psi_m), \tag{4}$$

where $V = |\dot{V}|$, the velocity amplitude of the mass vibration, and $A_{\mathrm{ext}} = |\dot{A}_{\mathrm{ext}}|$. If we choose Ψ_e so that

$$\mathrm{Im}\,(\Psi_e) = -\mathrm{Im}\,(\Psi_m)\,, \tag{5}$$

$\mathrm{Re}(\Psi_e)$ is maximized and is linked with V as

$$\mathrm{Re}\,(\Psi_e) = \frac{mA_{\mathrm{ext}}}{V} - \mu_m, \tag{6}$$

where μ_m is the mechanical damping of the proof mass. The sign of $\sqrt{(mA_{\mathrm{ext}}/V)^2}$ is chosen so as to allow $\mathrm{Re}(\Psi_e)$ to be non-negative. Injecting equation (6) into equation (2) we get

$$P_h = \frac{1}{2}V^2\left(\frac{mA_{\mathrm{ext}}}{V} - \mu_m\right) = \frac{1}{2}V\,(mA_{\mathrm{ext}} - \mu_m V)\,. \tag{7}$$

This expression has a maximum when $V = 0.5\ mA_{\mathrm{ext}}/\mu_m$, leading to an expression equivalent to the well-known formula for the maximal power provided by a non-ideal voltage source:

$$P_h = \tfrac{1}{8}(mA_{\mathrm{ext}})^2/\mu_m. \tag{8}$$

However, in practice, often the mass vibration is limited at $X_{\max}$ (by the position of the stoppers for instance). If $X_{\max} < 0.5\ \mathrm{mA_{ext}}/\mu_m$, we are in a so-called amplitude-constrained case [30], and the maximal velocity is $V = \omega X_{\max}$. To maximize the harvested power, the designer should choose this maximal velocity value to get as close as possible to the optimal V. From equation (7), this gives for the harvested power

$$P_h = \frac{1}{2}X_{\max}^2\omega^2\left(\frac{mA_{\mathrm{ext}}}{X_{\max}\omega} - \mu_m\right). \tag{9}$$

If μ_m is negligible as it was supposed in [30], we come to exactly the same formula for a *velocity-damped resonant generator* (VDRG) having a harmonic motion:

$$P_{h\max} = \tfrac{1}{2}X_{\max}\omega m A_{\mathrm{ext}} = \tfrac{1}{2}X_{\max}\omega^3 m X_{\mathrm{ext}}, \tag{10}$$

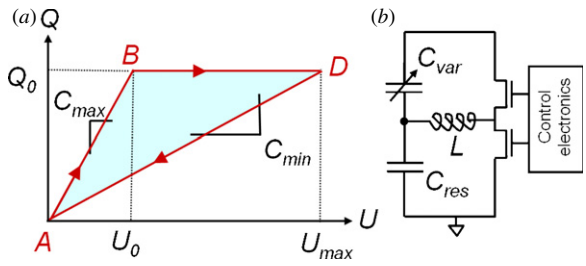

Figure 4. (*a*) Basic *Q*–*V* diagram of an electrostatic vibration energy harvester. (*b*) Possible circuit implementation (from [33]).

where X_{ext} is the displacement amplitude of the external vibrations, related to A_{ext} as $A_{\mathrm{ext}} = X_{\mathrm{ext}}\omega^2$.

This calculation of maximal power was carried out under a restrictive hypothesis of linearity of the load (i.e. the load is a linear dynamic system). However, it can be demonstrated that the load absorbs a maximal power only if it generates a sinusoidal force, i.e. only if the load is linear. The sufficient condition of the maximal power generation with a linear load is given by equations (5) and (6), either for a constrained displacement or not.

2.2. *Principle of an electrostatic harvester*

The idea of electrostatic energy harvesting is summarized in three steps: put an electrical charge Q_0 on a variable capacitor (C_{var}), when its capacitance is high ($C_{\max}$). Then reduce this capacitance to its minimal value $C_{\min}$, thanks to the motion due to mechanical vibrations, and eventually discharge the capacitor [33]. According to the formula of electrostatic co-energy stored in the capacitor $W = Q^2/(2\ C)$, the discharge energy is higher than the energy spent in charging the capacitor. The charge Q_0 on C_{var} being constant during the second phase of the process, this cycle generates an electrical energy given by

$$\begin{aligned}\Delta W &= W_{\mathrm{discharged}}(C_{\min}) - W_{\mathrm{charged}}(C_{\max}) \\ &= \frac{Q_0^2}{2}\left(\frac{1}{C_{\min}} - \frac{1}{C_{\max}}\right).\end{aligned} \tag{11}$$

The initial energy W_0 is put in the transducer when C_{var} equals $C_{\max}$, so it is equal to ${Q_0}^2/(2\ C_{\max})$ and equation (11) can be rewritten as

$$\Delta W = W_0\left(\frac{C_{\max}}{C_{\min}} - 1\right) = \frac{U_0^2}{2}C_{\max}\left(\frac{C_{\max}}{C_{\min}} - 1\right) \tag{12}$$

where U_0 is the initial voltage of the transducer corresponding to the charge Q_0. To obtain the power, $W_{h\max}$ should be multiplied by the frequency of the transducer's capacitance variation. The produced energy is $(C_{\max}/C_{\min} - 1)$ higher than the initially spend energy $\mathrm{W_0}$. The operation of such a system is illustrated by the charge–voltage (*Q*–*V*) diagram of the variable capacitor, the area ABD of the cycle being numerically equal to the generated energy (figure 4(*a*)). From the mechanical point of view, during this cycle the transducer generates on the mass an average damping force, tending to attenuate the vibrations.

The initial energy W_0 can be obtained by many ways. The most popular solution is the use of an electret layer, generally

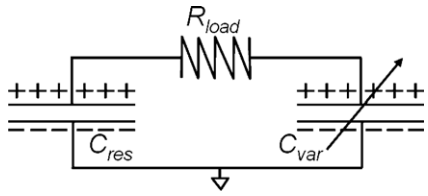

Figure 5. Typical architecture of a conditioning circuit without charge renewal.

located below the proof mass. Another possibility is to make a hybrid system which associates the electrostatic energy harvester with the use of a piezoelectric material [34]. Other techniques involve thermoelectric effect [35], or materials with different work functions [36].

2.3. Conditioning electronics for an electrostatic harvester

Compared with the amount of publications reported on the resonator/transducer block only a few studies address the surrounding electronics. The role of the conditioning circuit is the management of the charge flow on C_{var} following the principle described below and, as well, the management of the harvested power (accumulation, distribution to the load, etc). They can be classified into two categories, depending on their ability to renew or not the electrical charges on the reservoir capacitor. A typical architecture of a conditioning circuit without charge renewal is given in figure 5 [37]. Its operation is based on the hypothesis that the total amount of charge of C_{res} and C_{var} is constant during the whole operation. However, in practice, unavoidable leakage ends to deactivate completely this type of energy harvester. Conditioning circuits with charge renewal use the harvested energy to provide new charges to the reservoir capacitor from the electrical ground. If the energy consumed by the load is lower than the harvested energy, there is an increase of the electrical charge (and hence energy) on the reservoir capacitor: this allows accumulation and storage of the energy and gives a possibility of implementing a power management of the harvested energy. For this reason, our study focuses on a conditioning circuit belonging to the latter category.

The simplest triangular charge–constant Q–V cycle of figure 4(*a*) can be achieved using the analog conditioning circuit presented in figure 4(*b*) [33]. The inductor is used to transmit the energy between the large reservoir capacitor and the variable capacitor. The charge flow direction through the variable capacitor is then controlled by two switches, and this control has to be perfectly synchronized with the transducer variable capacitor planes motions. This synchronization issue is a major difficulty in the implementation of this kind of conditioning circuits. In [33], a programmable power controller circuit with digitally programmable delays was developed to define the on/off sequence of the switches. The operation of the controller supposed knowledge of the circuit operating condition, i.e. vibration frequency and initial phase of the vibrations. Obviously, such a requirement could not be satisfied in a real system, so in the same article the authors proposed an architecture allowing a feedback operation of the

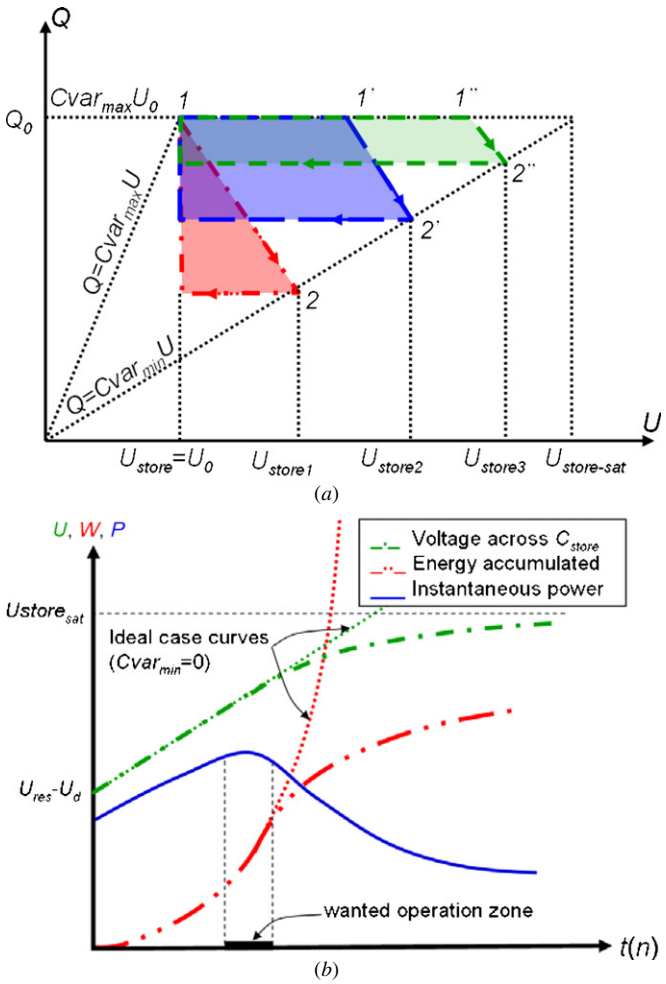

Figure 6. (*a*) Q–V diagram of the charge pump operation. (*b*) Evolution of voltage, energy and power across C_{store}.

controller and an automatic lock on the transducer capacitance variations but, as far as we know, no experimental validation of this concept has been provided so far. The main fundamental drawback of the harvesting scheme implemented by Meninger is that both switches have to be activated in every C_{var} variation cycle, with a very accurate timing to synchronize the charge flow with the C_{var} variation. Therefore, much energy is lost in the switch driving and in the detection of the moments at which C_{var} is maximal or minimal.

For this reason, an alternative architecture was proposed in 2006 by Yen *et al* [16], shown in figure 2. The idea is to introduce a third capacitor, called C_{store}, which accumulates the energy harvested in several consecutives cycles of C_{var} variations. Using a classical charge pump circuit, this can be done without using an inductor. After having accumulated some amount of energy in C_{store}, a flyback circuit is activated, and the harvested energy is transferred from C_{store} to C_{res} through an inductor, following the classical scheme for energy exchange between two capacitors. During the charge pumping, the new Q–V diagram is more complex than in [33]: it is composed of four zones, and at each following cycle the Q–V trajectory changes (figure 6(*a*)). This harvesting technique has the following advantages:

(1) The pump charge is auto-synchronized with the C_{var} variations thanks to the diodes D_1 and D_2, which play the role of switches. Thus, there is an energy economy on synthesizing the control signal at the vibration frequency.
(2) The flyback circuit is activated in each of n vibration cycles. A synchronization of switching is needed as well, but, differently to the initial scheme, if n is big enough, the time scale of the required precision is much larger than one vibration period, and no synchronization is needed with the oscillation phase of the resonator. Thus, the command circuitry is simpler and less energy is lost, since operating at a lower frequency.
(3) Only one electronics switch is needed, which greatly simplifies the electronics and substantially reduces the flyback losses.

In the same way as for the circuit in [33], the switch command should be implemented in a feedback with the energy state of the system, although the precision in timing is less stringent. In the work of B Yen, the switch is driven by a fixed periodic time sequence, which cannot be an appropriate solution for a real-life operation. Our preliminary theoretical and modeling studies reported in [38–40] highlighted that the switch should be ordered in function of the electrical state of the charge pump. It can be done by a smart block which senses U_{store} and U_{res} voltages and which generates the switching events following an appropriated algorithm [40].

2.4. Maximum power generation for the three capacitor scheme

The Q–V cycle in figure 6 changes at each oscillation. The diagram is bounded by the lines corresponding to $Q = C_{min}U_{var}$ and $Q = C_{max}U_{var}$ when n tends to infinity, which fixes the saturation voltage across U_{store} to $U_0 C_{max}/C_{min}$. Initially $U_{res} = U_{var} = U_{store} = U_0$, $C_{var} = C_{max}$ and the first cycle is triangular. However, the next cycles are trapezoidal. The cycle area, which is equivalent to the harvested energy, starts to increase with n. In the meantime the minimal charge on C_{var} increases, so the cycle becomes thinner and progressively degenerates to a pseudo line with a constant area when approaching the saturation voltage. Assuming that the vibrations are periodical, and each pump cycle takes exactly the same time, there is an operating mode at which the pump produces a maximum power, as shown qualitatively in figure 6(*b*).

To determine this maximal power, it is required to find the maximum of the following function:

$$\Delta W(n) = \Delta W_{1\to n} - \Delta W_{1\to n-1}, \tag{13}$$

where $\Delta_{W\to n}$ is the energy accumulated in C_{store} during n first pump cycles and is given by

$$\Delta W_{1\to n} = \frac{C_{res}C_{store}}{2(C_{res}+C_{store})}(U_{store\,n} - U_{res})^2 \approx \frac{C_{store}}{2}(U_{store_n} - U_{res})^2, \tag{14}$$

where U_{store_n} is the C_{store} voltage at the end of the nth cycle. The recurrent formula for U_{store_n} was derived in [16]:

$$U_{store\,n} = \frac{C_{store}}{C_{store}+C_{min}}U_{store\,n-1} + U_0\frac{C_{max}}{C_{store}+C_{min}}. \tag{15}$$

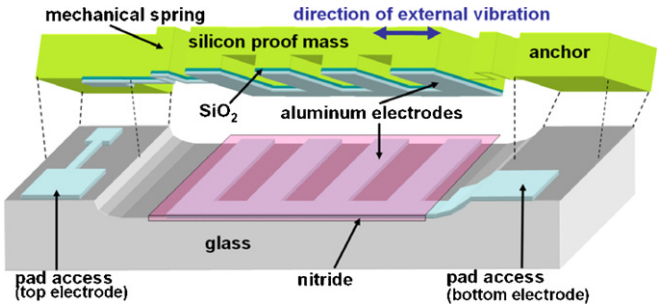

Figure 7. 3D schematic view of the harvester.

The quantity $\Delta W(n)$ in equation (13) has a maximum over n, but it cannot be found analytically. However, it is possible to find the maximum of $\Delta W(n)$ considering it as a function of $U_{store\,n}$, and find $U_{store\,n}$ at which ΔW_n is maximal. This can easily be done by looking for the maximum of the quadratic polynomial function defined by equations (13)–(15). We get for the optimal $U_{store\ n}$:

$$U_{store\_opt} = U_{res}\cdot\frac{\frac{C_{min}}{C_{store}} + \frac{C_{max}}{C_{min}} + 1}{\frac{C_{min}}{C_{store}} + 2}, \tag{16}$$

and

$$W_{n\ max} = \frac{U_{res}^2}{2}\cdot\frac{C_{min}\left(\frac{C_{max}}{C_{min}} - 1\right)^2}{\frac{C_{min}}{C_{store}} + 2}. \tag{17}$$

Usually $C_{store} \gg C_{min}$, so $W_{n\,max}$ is $2/(1 - C_{min}/C_{max})$ times lower than the maximal energy harvested in one cycle in the ideal triangular Q–V scheme of equation (12). If C_{max}/C_{min} and C_{store}/C_{min} are high, this factor tends to 2, which is consistent with equation (16) showing a twice lower maximal voltage across the transducer than for the case of the triangular harvesting scheme. However, when C_{max}/C_{min} is low, the harvester architecture of Yen is highly penalized compared to the ideal triangular harvesting scheme.

Note that none of these formulas take into account the drop voltage across the diodes. Equation (17) is a theoretical physical limit of the harvester that takes into account this specific electronics architecture, equation (12) gives the converted power for an ideal Q–V scheme, i.e. the maximal power that can be harvested from an electrostatic transducer.

3. Description of the fabricated transducer

3.1. Design and fabrication

A 3D schematic view of the batch-fabricated electrostatic transducer is given in figure 7. The proof mass is micromachined from a (1 0 0)-oriented, 380 μm thick single- and double-side polished 4 inch crystal silicon wafer, anodically bonded to a 500 μm thick glass substrate, and is designed to have an in-plane translational degree of freedom. The electrodes of the variable capacitance C_{var}, which are made of aluminum, are on the top-side glass and back-side silicon wafers respectively. The fabrication process is summarized as

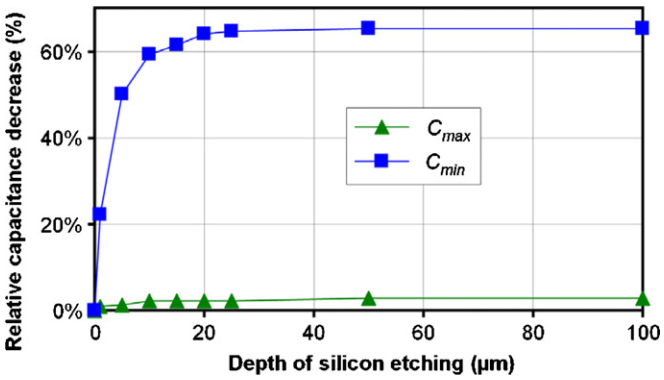

Figure 8. FEM simulation of a relative decrease of C_{var} versus depth of silicon partial backside etching between the aluminum patterns.

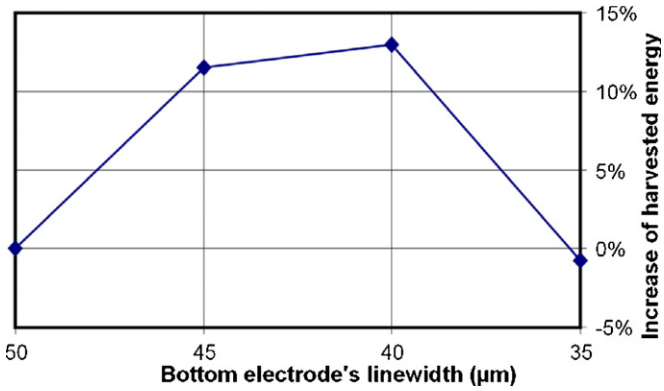

Figure 9. Evolution of maximal energy versus lower electrode line width, using equation (12) and FEM simulation results of C_{min} and C_{max} values.

follows. The glass wafer is patterned with gold used as a hard-mask material, and subsequently selectively etched with HF. Then the bottom electrode is patterned inside the glass cavities and covered with a nitride layer which provides a passivation layer acting against unwanted sticking. On the backside of the silicon wafer, a thermal oxide layer isolates the top electrodes from the substrate.

A large part of the minimal value of C_{var} is due to the overlap between the bottom electrode (on glass wafer) and the silicon area present between the aluminum lines of the top electrode [41]. We did FEM simulations (cf figure 8) that show a drastic decrease above 60% of this parasitic capacitance, if trenches of 20 μm are etched through this silicon material. Increasing the trench's depth above this value will not decrease C_{min}, probably because the fringe field effect will become dominant. In addition, this would reduce the mobile mass and increase the working frequency of the harvester. So, a mask made of PECVD (plasma enhanced chemical vapor deposition) nitride is deposited on the backside of the silicon wafer, and a 20 μm DRIE (deep reactive ion etching) is performed. A last hard mask is deposited on the topside of the silicon wafer for patterning the movable parts with a through wafer etching of 380 μm. Eventually, an anodic bonding is performed and the wafer is diced.

To obtain 380 μm thick beams with a width of 30 μm, smooth sidewalls, excellent anisotropy and very limited notching effect [42], we develop a three-step Bosh process using a RF/LF pulsed generator for the DRIE plasma reactor. First step consists in a classical SF_6/C_4F_8 RF biased etching through 200–250 μm of silicon. Then the time of SF_6 etching is increased to get rid of excessive polymer at the bottom of the patterns. When the aspect ratio-dependent etching (ARDE) effect could induce the notching effect, the RF biasing is turned into LF pulsed biasing.

At the end of the process, the gap between the top and bottom electrodes is 1.7 μm, including a nitride layer of 500 nm. Top electrode is made of 100 interconnected lines of 50 μm $\times$ 6.4 mm spaced with a gap of 50 μm. Figure 9 presents the normalized energy using equation (12) versus various lower electrode's line widths, for a given initial voltage U_0 and FEM simulations of C_{min} and C_{max} configurations. This shows an optimal width of 40 μm due to fringed field effects. With all these design parameters, the capacitance is expected to vary between 145 pF and 79 pF.

Electrical connections toward the conditioning circuit are obtained thanks to large openings in the silicon wafer, which allows wire bonding on the aluminum electrodes deposited on the glass wafer. An electrical contact between the electrodes on the backside of the silicon wafer and the topside of the glass wafer is obtained by the mechanical pressure of the two aluminum layers during anodic bonding.

3.2. AC response of the harvester

In order to perform the measurements, the resonators were glued on a PCB, and wire bonded to gold pins electrically connected to the conditioning electronics circuit with soft wires. The PCB is screwed to the in-plane vibration excitation table (figure 10).

The quality factor of the resonator was measured indirectly, by applying a dc+ac voltage to the electrodes of the capacitive transducer, and by sensing with a transimpedance amplifier the electrical current produced by the mechanical displacement of the transducer's electrodes [43, 44]. The transmission curve is shown in figure 11. The measured resonance frequency is 250.5 Hz and the -3 dB bandwidth is 1.7 Hz, which corresponds to a quality factor of 147. This experience provides Q in low amplitude mode, since the mechanical force generated by the electrostatic transducer with the used voltage levels was weak. In the large amplitude mode which is needed for efficient energy harvesting, due to the not fully linear stretching of the springs, the -3 dB bandwidth increases to 2.5 Hz, which corresponds to a Q of 100.

3.3. Dynamic characterization of the capacitance

A dynamic measurement of C_{var} is achieved by measuring the phase shift in a RC_{var} circuit powered with an ac voltage at a higher frequency than the applied external vibrations (cf figure 12). The capacitance is calculated as

$$C_{var} = \frac{1}{\tan(\theta) R\omega}, \tag{18}$$

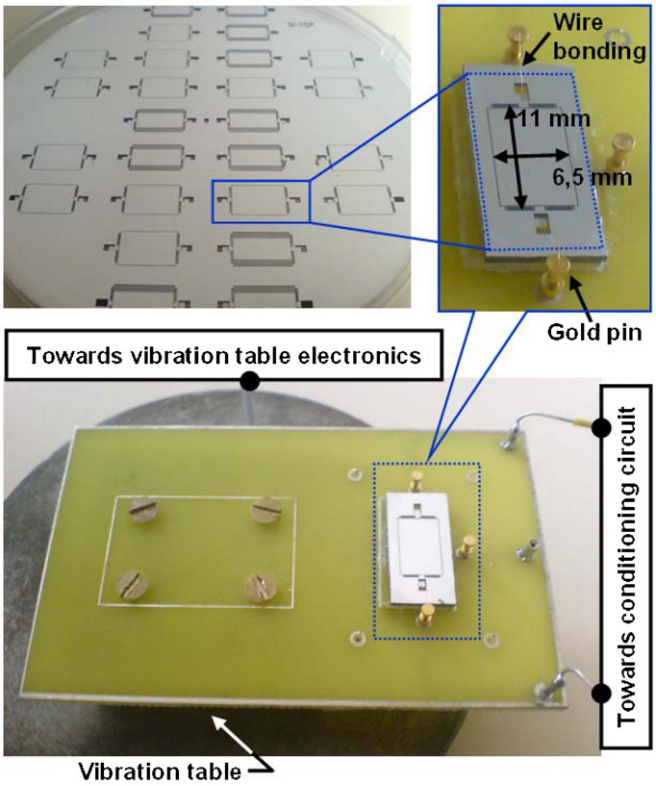

Figure 10. Pictures of fabricated devices and test bench.

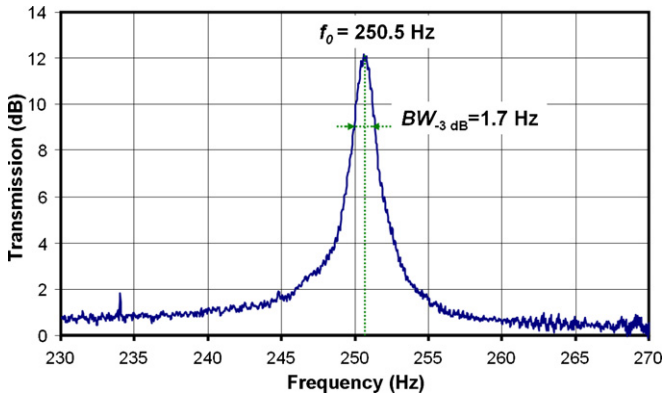

Figure 11. AC response of the resonator in low amplitude mode after subtraction of its parasitic coupling capacitance. The transmission corresponds to the ratio of the output motional current with the ac input voltage applied on the transducer, times the transresistance of the output amplifier.

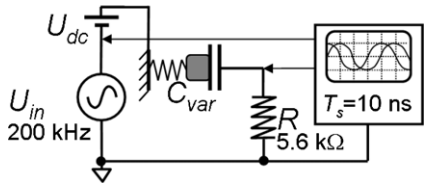

Figure 12. Setup for the dynamic measurement of the transducer's capacitance.

where ω is the angular frequency of the source signal, θ is the phase shift between the voltage across the capacitor and the voltage generated by the source. R and ω have to be chosen so as to maximize the accuracy of C_{var} measurement. The precision of θ measurement is defined by the resolution of the used oscilloscope, i.e. by the sampling period T_s. The time error being T_s, the error on θ is $T_s\omega$. Considering that R is known with a negligible error, we have the following error on C_{var}:

$$\Delta C_{\text{var}} = d\left(\frac{1}{\tan(\theta)\, R\omega}\right) = -\frac{1}{R\omega}\frac{1}{\sin^2(\theta)}\,\mathrm{d}\theta$$
$$= -C_{\text{var}}\frac{1}{\cos(\theta)\sin(\theta)}\frac{\mathrm{d}\theta}{\mathrm{d}t}\,\mathrm{d}t, \tag{19}$$

where $\mathrm{d}t$ is the time error measurement. For finite error, if $\mathrm{d}t = T_s$, it gives

$$\frac{\Delta C_{\text{var}}}{C_{\text{var}}} = -2\frac{T_s\omega}{\sin(2\theta)}. \tag{20}$$

To minimize the error, a phase shift of $\pi/4$ should be chosen. This is only possible if the exact value of C_{var} is known *a priori*. Since we know the range of the expected values from design, we adjust ω and R so as to maximize the measurement accuracy at the C_{var} mean value $C_{\text{var\_}m}$. The governing ratio is

$$C_{\text{var\_}m} R\omega = 1, \tag{21}$$

which leaves one free parameter among ω and R. But the choice of the frequency is constrained by two factors. Firstly, the frequency ω should be much higher than the frequency of the capacitance variation. This is necessary for the circuit to operate in quasi-stationary sinusoidal mode in which the above analysis is valid. On the other hand, the available oscilloscope memory is finite, which limits the maximal acquisition time: a high frequency prohibits long data acquisition time, and thus makes difficult the observation of a long-term capacity evolution. Therefore, a compromise is necessary. From equations (18) and (20), the relative error can be calculated as

$$\frac{\Delta C_{\text{var}}}{C_{\text{var\_}m}} = -2\frac{T_s\omega}{\sin\left[2a\tan\left(\frac{1}{\omega R C_{\text{var\_}m}}\right)\right]}. \tag{22}$$

Thus, for each measurement, the above formula must be applied *a posteriori* on the maximal and minimal measured values of C_{var} to estimate the worse-case error.

The in-plane vibrations are applied at the device mechanical resonance, i.e. 250 Hz, with a maximum acceleration of 0.25 g and a magnitude of the proof mass displacement of 50 μm. The frequency of the ac voltage is set to 200 kHz. The measurements have been performed with an oscilloscope having a sampling time T_s of 10 ns and with a resistance R of 5.6 kΩ. If only a weak sinusoidal voltage is applied on C_{var}, it exhibits a variation from 73 to 144 pF as shown in figure 13(*a*), which is very close to the expected values. Equation (22) gives a maximum relative error below 3.1%. During one mechanical cycle, the proof mass passes twice through the mean position, so the frequency of C_{var} variation is consequently twice the mechanical vibration frequency. However, when a dc voltage U_{dc} is superposed on the sinusoidal voltage U_{in} (figure 12), the vertical electrostatic force between the top and bottom electrodes pulls the proof mass down to the substrate and thus

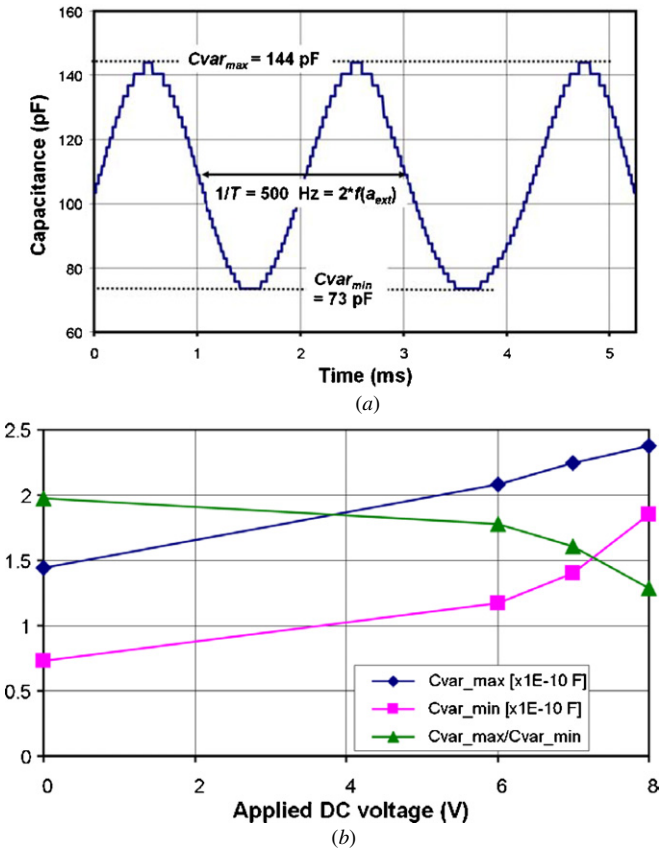

Figure 13. Dynamic measurement of the transducer's capacitance: (*a*) capacitance variation C_{var} with time with no dc voltage applied, (*b*) measurement of $Cvar_{\max}$, $Cvar_{\min}$ and $Cvar_{\max}/Cvar_{\min}$ ratio with applied increasing applied dc voltage.

Table 1. Characteristics of the transducer.

Characteristics	value
Dimensions	$11 \times 6.5 \times 0.86$ mm^3
In-plane resonance frequency	250 Hz
Min/max capacitance	73 pF/144 pF
Out-of-plane resonance frequency	3521 Hz (simulated)
Quality factor (low/large amplitude mode)	147/100
Proof mass	46.1 mg
Min. acceleration for full-range displacement	0.1 *g*
Out-of-plane instability voltage	12 V

reduces the ratio $C_{\max}/C_{\min}$, mainly because of an increase of the fringe field responsible for $C_{\min}$ value. Thus, at U_{dc} = 8 V, the measured ratio $C_{\max}/C_{\min}$ is 1.3 (cf figure 13(*b*)). This corresponds to a gap reduction of about 40%. The main characteristics of the tested device are given in table 1.

4. Measurement of converted power

4.1. Description of the method

To demonstrate an electromechanical power conversion, the following experience is carried out using the experiment diagram presented in figure 14. Ultra-low-leakage amplifiers

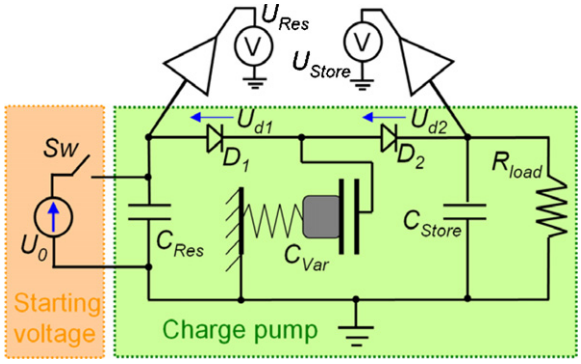

Figure 14. Schematic of the charge pump circuit used for testing the transducer.

allow a precise U_{res} and U_{store} measurement. The C_{var} capacitor is submitted to external vibrations close to the resonance frequency of the resonator, so that C_{var} varies in time. The switch *Sw* is switched on at the beginning of the experiment. Once the capacitors are charged, the switch *Sw* is switched off, and from this moment t_0 the network operates in autonomous mode. Then the energy sources in the circuit are the discharging C_{res} and C_{store} capacitors and the electromechanical transducer which converts vibration energy into electrical domain (the energy of C_{var} is negligible since C_{var} is small as compared to C_{res} and C_{store}). The energy is consumed by the load resistance and the diodes. At each moment the corresponding power balance equation is expressed as

$$P_{\text{mec}} + P_{C_{\text{res}}} + P_{C_{\text{store}}} = P_{R_{\text{load}}} + P_{\text{diodes}}. \tag{23}$$

The goal of this experiment is to measure the electrical terms of equation (23) and to deduce P_{mec} from it. The straightforward way to measure the electrical power is to measure the evolution of the instantaneous voltages on the three capacitors. However, it is difficult to measure the voltage on the small capacitance C_{var} without perturbing the circuit operation. Instead, we measure the slow evolution of the voltages on C_{res} and C_{store}, and calculate the average mechanical power produced during $\Delta t = 6$ s after t_0.

The energy provided by the capacitors is calculated as

$$W_C = \frac{C}{2}\left[U_C^2(t_0) - U_C^2(t_0 + \Delta t)\right], \tag{24}$$

and the energy consumed by the load is calculated as

$$W_R = \int_{t_0}^{t_0+\Delta t} \frac{U_{\text{store}}^2(t)}{2R_{\text{load}}}\,\mathrm{d}t. \tag{25}$$

The energy consumed by the diodes is indirectly calculated from the charge evolution on C_{res}. On average, C_{var} does not consume any charge. Then all the charges leaving C_{res} flue through the diodes and the load toward the ground and the energy dissipated in one diode is

$$W_d = U_d Q(t_0, t_0 + \Delta t) = U_d C[U_C(t_0) - U_C(t_0 + \Delta t)], \tag{26}$$

where $Q(t_0, t_0+\Delta t)$ is the charge lost by C_{res} between t_0 and $t_0+\Delta t$, U_d is the diode threshold voltage. Equation (26) is

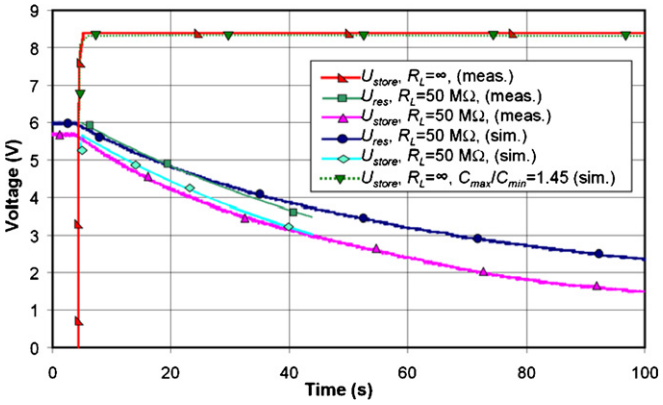

Figure 15. Measurements and theoretical evolutions with time of V_{res} and V_{store}, with and without a resistive load.

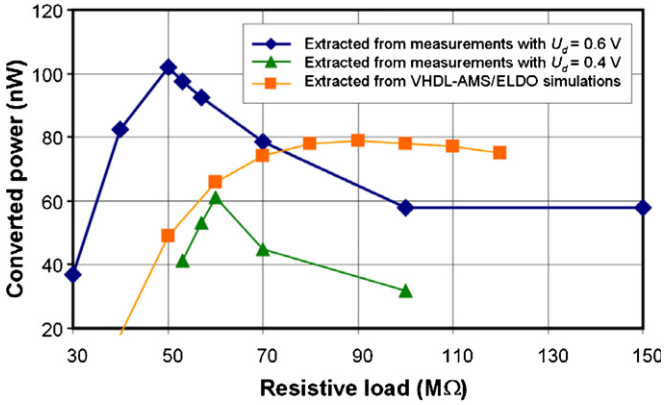

Figure 16. Harvested power versus the resistive load.

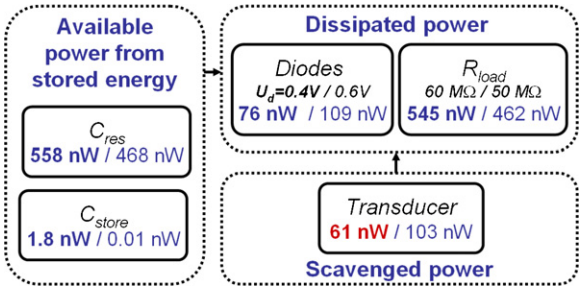

Figure 17. Power balance diagram of the system extracted from experimental data over a time period of 20 s and with optimum loads for two values of V_d.

based on the hypothesis that U_d is constant, which is not exactly the case. For our calculations we take $U_d = 0.4$ V and 0.6 V. The first value is consistent with indirect measurement and confirmed by the simulation. It corresponds to the typical average currents circulating in our system, which transfers the essential amount of charges.

In our experiment the system is pre-charged with $U_0 = 6$ V, corresponding to approximately half of the out-of-plane pull-in voltage: thus, at each period of C_{var} variation, the charge pump transfers the charge amount $(C_{\max} - C_{\min})U_0 \sim 420$ pC from C_{res} toward C_{store}, which corresponds to a mean current of ∼210 nA. The parasitic leakage currents need to be much smaller in order to perform accurate measurements. We used JPAD5-E3 diodes which contribute with only 5 pA of leak. The voltage measurement circuit contributes with a leakage current of 250 fA.

4.2. Results

Figure 15 shows the voltage evolutions of U_{res} and U_{store} with and without a resistive load of 50 MΩ. The measurement without the load identifies the saturation voltage of the charge pump $U_{\text{store\_sat}}$ to be 8.4 V (figure 15, curve on top). From the theory,

$$U_{\text{store\_sat}} = \frac{C_{\max}}{C_{\min}}(U_0 - U_d) - U_d, \qquad (27)$$

which is nearly 8.45 V for $C_{\max}/C_{\min} = 1.45$ and $U_d = 0.1$ V. Such a low diode voltage is explained by the fact that there is nearly no charge transfer when the charge pump is saturated.

To evaluate the part of the power which is harvested from the mechanical domain, we performed experiments with various loads from 30 to 150 MΩ. A typical example of the obtained curves is given in figure 15 for $R_{\text{load}} = 50$ MΩ. This experiment was modeled using the VHDL-AMS model presented in [38] implemented with the same $C_{\max}/C_{\min}$ ratio of 1.45 and with a realistic exponential diode model. For the capacitor voltage evolution, the modeling and the experiment agreed better than 3%.

The plot in figure 16 shows the value of P_{mec} calculated from the measured and from the simulated voltage evolutions. When the power dissipated in the diodes is calculated from equation (26), with $U_d = 0.4$ V/0.6 V assumed constant, we obtain a maximal electrical power generation of 61/103 nW on a 60/50 MΩ load resistor. The related power balance is shown in figure 17. The power extracted from the modeling experiments highlights a maximal power of 79 nW for an optimal load of 90 MΩ. This discrepancy results from the difficulty to account correctly for the diode losses in the calculation of the experimental power.

We calculate the maximal convertible power in the conditions of our experiment using the formula of equation (17). With $C_{\max}$ and $C_{\min}$ values taken from the plot in figure 13(*b*) for the maximum transducer voltage of 8 V, $C_{\text{store}} = 3$ nF and $V_{\text{res}} = 5.6$ V (we subtract the 0.4 V drop voltage of the diode $D1$ from U_0), equation (17) gives the maximal harvested energy by cycle of 0.12 nJ, which, once multiplied by twice the mechanical vibration frequency of 250 Hz, gives 59 nW. This fits perfectly the results of our experiment.

5. Conclusion

A silicon-based electrostatic vibration energy harvester fabricated in a batch process has been presented. We have shown experimentally its ability to scavenge mechanical vibration energy without using an electret layer. After a precharge of the transducer at 6 V, the measurements have been performed in autonomous mode and the converted power is 61 nW, with external vibrations at 250 Hz and an acceleration amplitude of 0.25 g. The −3 dB bandwidth of the resonator

Table 2. Comparison of electrostatic energy harvesters.

Author [reference]	Year	Operating frequency f (Hz)	Device area A (mm^2)	Operation voltage (V)	Converted power P_h (μW)	Figure of merit (FOM) $P_h/(U^2 fA)$, (10^8 μW/(mm^2 Hz V^2)$^{-1}$)
Despesse *et al* [5]	2005	50	1800	120	1050	80
Yen *et al* [16]	2006	1560	4356	6	9.47[a]	4
Tsutsumino *et al* [20]	2006	20	200	950 (electret)	37.7	1
Ma *et al* [45]	2007	4100	25.9	15 ('electret like')	0.065	0.3
Suzuki *et al* [22]	2008	37	234	450 (electret)	0.28	2×10^{-3}
This work [27]	2008	250	66	8	0.061	6
Hoffmann [46]	2008	1460	30	50	3.8	4

[a] The authors provide only the power delivered to the load (1.8 μW), and they note that the efficiency is about 19%. Thus, to roughly estimate the converted power, we divided 1.8 μW by 0.19.

is 2.5 Hz in large amplitude mode and is 1.7 Hz in low amplitude mode, so the external vibration frequency has to match its mechanical resonance with a good accuracy in order to harvest significant power. The total volume of the transducer, including the bonding pads, is below 1 cm^2 $\times$ 1 mm.

Given the initial voltage of C_{res} and the available range of the transducer capacitance variations, we demonstrated the conversion of the maximal amount of power of 61 nW. If we compare these results with the maximal power that can be obtained with an optimal electrostatic transduction scheme with the same V_{res}, $C_{\max}$ and $C_{\min}$ (equation (12)), the efficiency of our harvester is about 10%, which is consistent with the low $C_{\max}/C_{\min}$. Considering the available mechanical power calculated with equation (10), the efficiency falls to 1.5%. In fact, equation (10) takes into account only the spring-mass system, and considers an 'ideal' transducer without accounting for the transduction mechanism. These low efficiencies are common with these kinds of devices and it shows that there is a lot of room to improve an electrostatic VEH. Since in electrostatic transducers, the harvested power is proportional to the square of the voltage across the variable capacitance, for our system the V_{res} voltage should be in the range of tens of volts to fully benefit our transducer capabilities. This illustrates that the main issue for the electrostatic VEH is its more immunity to the pull-in instability than the increase of the resonator's mass.

The converted power of our device is lower than some figures that can be found in the literature. However, an adequate comparison with the existing works implies as well a consideration of other factors like size, operating voltage and condition of experience. For example, the power of 1.8 mW delivered to load reported by Yen was obtained with a transducer capacitor built with large square aluminum and steel sheets of 6.6 cm side and at a frequency of 1.5 kHz. Our structure is 30 times smaller in area, and operates at a frequency seven times lower, which is more realistic for the practical applications. So, to make an adequate comparison of our work with other VEH, we propose a simple figure of merit (FOM) defined as a normalized converted power:

$$\text{FOM} = \frac{P_h}{U^2 f S}, \tag{28}$$

where P_h is the power converted from the mechanical to the electrical domain, U is the maximal voltage applied on the capacitive transducer, f is the external vibration frequency and S is the device area. Indeed, from equation (11) we can note that the output power of capacitive harvesters is proportional to the square of the pre-charge voltage, to the frequency and to the maximal transducer capacitance value. The latter is more or less directly proportional to the device area. This FOM works also with transducers using electret, but few publications give the voltage across the variation capacitance terminals. Table 2 presents the calculation of this FOM for several published works.

Acknowledgments

This work has been partially funded by the French National Research Agency (ANR) through the contract JC05-54551 and is supported by the French competitiveness cluster Advan*City*.

References

[1] Roundy S 2003 Energy scavenging for wireless sensor nodes with a focus on vibration to electricity conversion *PhD Thesis* University of California Berkeley

[2] Paradiso J A and Starner T 2005 Energy scavenging for mobile and wireless electronics *IEEE Pervasive Comput.* **4** 18–27

[3] Veld B O H, Hohlfeld D and Pop V 2009 Harvesting mechanical energy for ambient intelligent devices *Inf. Syst. Front. Arch.* **11** 7–18

[4] Roundy S, Wright P K and Rabaey J 2003 A study of low level vibrations as a power source for wireless sensor nodes *Proc. Comput. Commun.* **26** 1131–44

[5] Despesse G, Jager T, Chaillout J J, Léger J M, Vassilev A, Basrour S and Charlot B 2005 Fabrication and characterization of high damping electrostatic micro devices for vibration energy scavenging *Proc. DTIP'05* pp 386–90

[6] Löhndorf M *et al* 2007 Evaluation of energy harvesting concepts for tire pressure monitoring systems *Proc. PowerMEMS2007 (Freiburg, Germany)* pp 331–4

[7] Depriest J 2000 Aircraft engine attachment and vibration control *SAE Trans.* **109** 217–27

[8] Glynne-Jones P, Tudor M J, Beeby S P and White N M 2004 An electromagnetic vibration-powered generator for intelligent sensor systems *Sensors Actuators* A **110** 344–9

[9] Beeby S P, Torah R N, Tudor M J, Glynne-Jones P, O'Donnell T, Saha C R and Roy S 2007 A micro electromagnetic

generator for vibration energy harvesting *J. Micromech. Microeng.* **17** 1257–65
[10] Roundy S and Wright P K 2004 A piezoelectric vibration based generator for wireless electronics *Smart Mater. Struct.* **13** 1131–42
[11] Marzencki M, Ammar Y and Basrour S 2008 Integrated power harvesting system including a MEMS generator and a power management circuit *Sensors Actuators* A **145–146** 363–70
[12] Renaud M, Karakaya K, Sterken T, Fiorini P, Van Hoof C and Puers R 2008 Fabrication, modelling and characterization of MEMS piezoelectric vibration harvesters *Sensors Actuators* A **145–146** 380–86
[13] Garbuio L, Lallart M, Guyomar D, Richard C and Audigier D 2009 Mechanical energy harvester with ultra low threshold rectification based on SSHI non-linear technique *IEEE Trans. Ind. Electron.* **56** 1048–56
[14] Miao P, Mitcheson P D, Holmes A S, Yeatman E M, Green T C and Stark B H 2006 MEMS inertial power generators for biomedical applications *Microsyst. Technol.* **12** 1079–83
[15] Kiziroglou M E, He C and Yeatman E M 2009 Rolling rod electrostatic microgenerator *IEEE Trans. Ind. Electron.* **56** 1101–8
[16] Yen B C and Lang J H 2006 A variable capacitance vibration-to-electric energy harvester *IEEE Trans. Circuits Syst.* **53** 288–95
[17] Wang L and Yuan F G 2007 Energy harvesting by magnetostrictive material (MsM) for powering wireless sensors in SHM *Proc. SPIE 14th Int. Symp. on Smart Structures and Materials & NDE and Health Monitoring (SSN'07)*
[18] Dong S, Zhai J, Li J F, Viehland D and Priya S 2008 High power density magnetoelectric energy harvester *Proc. 17th IEEE Int. Symp. on the Applications of Ferroelectrics (ISAF'08)* vol 1 pp 1–2
[19] Lo H S and Tai Y C 2008 Parylene-HT-based electret rotor generator *Proc. IEEE (MEMS'08)* pp 984–7
[20] Tsutsumino T, Suzuki Y, Kasagi N and Sakane Y 2006 Seismic power generator using high-performance polymer electret *Proc. IEEE (MEMS'06)* pp 98–101
[21] Sterken T, Fiorini P, Altena G, Van Hoof C and Puers R 2007 Harvesting energy from vibrations by a micromachined electret generator *Proc. Transducers'07* pp 129–32
[22] Suzuki Y, Edamoto M, Kasagi N, Kashwagi K and Morizawa Y 2008 Micro electrets energy harvesting device with analogue impedance conversion circuit *Proc. PowerMEMS'08* pp 7–10
[23] Naruse Y, Matsubara N, Mabuchi K, Izumi M and Honma K 2008 Electrostatic micro power generator from low frequency vibration such as human motion *Proc. PowerMEMS'08* pp 19–22
[24] Tashiro R, Kabei N, Katayama K, Ishizuka Y, Tsuboi F and Tsuchiya K 2000 Development of an electrostatic generator that harnesses the motion of living body *JSME Int. J.* C **43** 916–22
[25] Myazaki M, Tanaka H, Ono G, Nagano T, Ohkubo N, Kawahara T and Yano K 2003 Electric-energy generation using variable capacitive resonator for power-free LSI: efficient analysis and fundamental experiment *Proc. Int. Symp. on Low Power Electron. Design* pp 193–8
[26] Mizumo M and Chetwynd D G 2003 Investigation of a resonance microgenerator *J. Micromech. Microeng.* **13** 209–16
[27] Paracha A M, Basset P, Galayko D, Dudka A, Marty F and Bourouina T 2008 Characterization of a DC/DC converter using an in-plane bulk silicon capacitive transducer for vibration-to-electricity power conversion *Proc. 8th Int. Workshop on Micro and Nanotechnol. for Power Generation and Energy Conv. Appl. (PowerMEMS'08)*
[28] Paracha A M, Basset P, Galayko D, Dudka Adrei, Marty F and Bourouina T 2009 MEMS DC/DC converter for 1D and 2D vibration-to-electricity power conversion *Proc. 15th Int. Conf. on Solid-State Sensors, Actuators and Microsystems (Transducers'09)* pp 2098–101
[29] Williams C B and Yates R B 1996 Analysis of a micro-electric generator for microsystems *Sensors Actuators* A **52** 8–11
[30] Mitcheson P D, Green T C, Yeatman E M and Holmes A S 2004 Architectures for vibration-driven micropower generators *IEEE J. MEMS* **13** 429–40
[31] Beeby S P, Tudor M J and White N M 2006 Energy harvesting vibration sources for microsystems applications *Meas. Sci. Technol.* **17** 175–95
[32] Mitcheson P D, Yeatman E M, Rao G Kondala, Holmes A S and Green T C 2008 Energy harvesting from human and machine motion for wireless electronic devices *Proc. IEEE* **96** 1457–86
[33] Meninger S, Mur-Miranda J O, Amirtharajah R, Chadakasan A P and Lang J H 2001 Vibration-to-electric energy conversion *IEEE Trans. Very Large Scale Integr. (VLSI) Syst.* **9** 64–76
[34] Khbeis M *et al* 2006 Design of a hybrid ambient low frequency, low intensity vibration energy scavenger *Proc. PowerMEMS'06* pp 287–90
[35] Sato N, Ishii H, Urano M, Sakata T, Terada J, Morimura H, Shigematsu S, Kudou K, Kamei T and Machida K 2006 Novel MEMS power generator with integrated thermoelectric and vibrational devices *Proc. Transducers 2005* pp 295–8
[36] Kuehne M, Frey A, Marinkovic D, Eckstein G and Seidel H 2006 A capacitive vibration-to-electrical energy converter with built-in voltage *Sensors Actuators* A **142** 263–9
[37] Mitcheson P D, Sterken T, Yeatman E M, He C, Kiziroglou M and Puers R 2008 Electrostatic microgenerators *Meas. Control* **41** 114–9
[38] Galayko D, Pizarro R, Basset P, Paracha A M and Amendola G 2007 AMS modeling of controlled switch for design optimization of capacitive vibration energy harvester *Proc. IEEE Int. Behavioral Modeling and Simulation Conf. (BMAS'07)* pp 115–20
[39] Galayko D, Pizarro R, Basset P, Paracha A M and Amendola G 2007 Optimization and AMS modeling of capacitive vibration harvester *Proc. 7th Int. Workshop on Micro and Nanotechnol. for Power Generation and Energy Conv. Appl. (PowerMEMS'07) (Freiburg, Germany)* pp 109–12
[40] Galayko D and Basset P 2008 Mechanical/electrical power-aware impedance matching for design of capacitive vibration energy harvesters *Proc. 8th Int. Workshop on Micro and Nanotechnol. for Power Generation and Energy Conv. Appl. (PowerMEMS'08)*
[41] Parracha A M, Basset P, Marty F, Chasin A Vaisman, Poulichet P and Bourouina T 2007 A high power density electrostatic vibration-to-electric energy converter based on an in-plane overlap plate (IPOP) mechanism *Proc. 9th Symp. on Design, Test, Integration and Packaging Conf. (DTIP'07)*
[42] Marty F, Rousseau L, Saadany B, Mercier B, Francais O, Mita Y and Bourouina T 2005 Advanced etching based on deep reactive ion etching for silicon high aspect ratio microstructures and three dimensional micro and nano structures *Microelectron. J.* **36** 673–7

[43] Galayko D 2002 Microelectromechanical thick-film polysilicon micromachined filters and their applications in the intermediate frequency filtering *PhD Dissertation* University of Lille (in French)

[44] Nguyen Clark T C 1994 Mecromechanical signal processors *PhD Dissertation* University of California Berkeley

[45] Ma W, Zhu R, Rufer L, Zohar Yitshak and Wong M 2007 An integrated floating-electrode electric microgenerator *J. Microelectromech. Syst.* **16** 29–37

[46] Hoffmann D, Folkmer B and Manoli Y 2008 Fabrication and characterization of electrostatic micro-generators *Proc. 8th Int. Workshop on Micro and Nanotechnol. for Power Generation and Energy Conv. Appl. (PowerMEMS'08)*